

## OVAL SHAPED DROPLET SOLUTIONS IN THE SATURATION PROCESS OF SOME PATTERN FORMATION PROBLEMS\*

XIAOFENG REN<sup>†</sup> AND JUNCHENG WEI<sup>‡</sup>

**Abstract.** The first stage in the transition from a coarse structure to a fine structure in many pattern formation problems involves the change of a standard geometric object such as a round disc to a less standard geometric object such as an oval shaped set. On a generic domain two small oval shaped sets are found as solutions to a nonlocal geometric problem. This problem arises as the singular limit of both the Ohta–Kawasaki theory for diblock copolymers and the Gierer–Meinhardt theory for morphogenesis in cell development. The two sets have the same center, which is a global minimum of the diagonal of the regular part of a Green’s function. This minimum point may be regarded as a kind of center of the domain. Moreover the second derivatives of the regular part of the Green’s function define a major axis and a minor axis for the domain. One of the oval shaped solutions is stable and aligns itself along the major axis. The other oval shaped solution is unstable and is parallel to the minor axis.

**Key words.** oval droplet, saturation, major axis, minor axis, diblock copolymer morphology, morphogenesis, regular part of Green’s function

**AMS subject classifications.** 34E10, 82D60

**DOI.** 10.1137/080742361

**1. Introduction.** Fine, periodic structures are often preferred to coarse, single structures in many pattern formation problems. Examples include the Ohta–Kawasaki density functional theory for block copolymers [13] and the Gierer–Meinhardt theory for morphogenesis in cell development [6]. In the the Ohta–Kawasaki theory, the level of structure saturation is controlled by the strength of the long-range interaction between polymer chains. In the Gierer–Meinhardt theory, the diffusion coefficient of the inhibitor performs the same function.

The transition from a coarse structure to a fine structure is not well understood mathematically. Such a saturation process may contain several steps. As depicted in Figure 1, first a well-known single object, like a round disc, deforms to a less standard structure, such as an elongated, oval shaped set. Then deformation continues and a neck appears on the set signaling splitting. Finally the structure breaks off into two disjoint pieces.

Our study uses a nonlocal geometric model. We are given a smooth and bounded domain  $D$  in  $R^2$  and two parameters  $a \in (0, 1)$  and  $\gamma > 0$ . To each subset  $E$  of  $D$  with the prescribed size  $|E| = a|D|$ , where  $|E|$  and  $|D|$  are the Lebesgue measures of  $E$  and  $D$ , respectively, we associate a free energy by

$$(1.1) \quad J(E) = P_D(E) + \frac{\gamma}{2} \int_D |(-\Delta)^{-1/2}(\chi_E - a)|^2 dx.$$

---

\*Received by the editors December 2, 2008; accepted for publication (in revised form) July 10, 2009; published electronically September 9, 2009.

<http://www.siam.org/journals/siap/70-4/74236.html>

<sup>†</sup>Corresponding author. Department of Mathematics, George Washington University, Washington, DC 20052 (ren@gwu.edu). This author’s research was supported in part by NSF grants DMS-0509725, DMS-0754066, and DMS-0907777.

<sup>‡</sup>Department of Mathematics, Chinese University of Hong Kong, Hong Kong, People’s Republic of China (wei@math.cuhk.edu.hk). This author’s research was supported in part by an earmarked grant of RGC of Hong Kong.

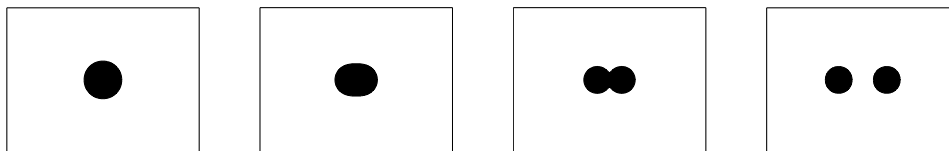


FIG. 1. A round droplet deforms to an oval droplet and then to a necked droplet, before splitting into two droplets.

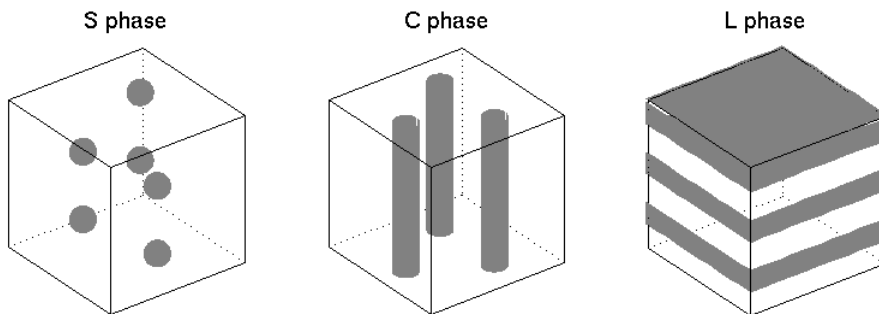


FIG. 2. The spherical, cylindrical, and lamellar morphology phases commonly observed in diblock copolymer melts. The dark color indicates the concentration of type A monomers, and the white color indicates the concentration of type B monomers.

Here  $P_D(E)$  is the perimeter of the part of the boundary of  $E$  that is inside  $D$ , i.e., the total length of the curves  $\partial E \cap D$ . The characteristic function  $\chi_E$  of  $E$  is defined by  $\chi_E(x) = 1$  if  $x \in E$  and  $\chi_E(x) = 0$  if  $x \in D \setminus E$ . The most interesting part in (1.1) is the nonlocal operator  $(-\Delta)^{-1/2}$ . From the  $-\Delta$  operator on  $D$  with the Neumann boundary condition on  $\partial D$ , one obtains its inverse,  $(-\Delta)^{-1}$ , which is a nonlocal operator applied to functions on  $D$  with zero average, such as  $\chi_E - a$ . Our  $(-\Delta)^{-1/2}$  is the positive square root of the operator  $(-\Delta)^{-1}$ .

If a subset  $E$  of  $D$ , satisfying  $|E| = a|D|$ , is a critical point of  $J$  and  $\partial E \subset D$ , there exists a number  $\lambda$  such that

$$(1.2) \quad H(\partial E) + \gamma(-\Delta)^{-1}(\chi_E - a) = \lambda \quad \text{on } \partial E.$$

The constant  $\lambda$  is a Lagrange multiplier from the constraint  $|E| = a|D|$ , and  $H(\partial E)$  is the curvature of the curve  $\partial E$  viewed from  $E$ .

Equation (1.2) arises from several problems. One of them is the Ohta-Kawasaki theory for diblock copolymers. In a diblock copolymer a molecule is a linear chain of an A-monomer block grafted covalently to a B-monomer block [1]. This results in local microphase separation: microdomains rich in A monomers and microdomains rich in B monomers appear to form morphological phases. Figure 2 shows the spherical, cylindrical, and lamellar phases.

The free energy of a diblock copolymer melt proposed by Ohta and Kawakaki can be written on a bounded domain as

$$(1.3) \quad I(u) = \int_D \left[ \frac{\epsilon^2}{2} |\nabla u|^2 + W(u) + \frac{\epsilon\gamma}{2} |(-\Delta)^{-1/2}(u - a)|^2 \right] dx.$$

The relative density of the A monomers is  $u$ ; the relative density of the B monomers is  $1 - u$ . The function  $W$  is a balanced double well potential such as  $(1/4)u^2(1 - u)^2$ .

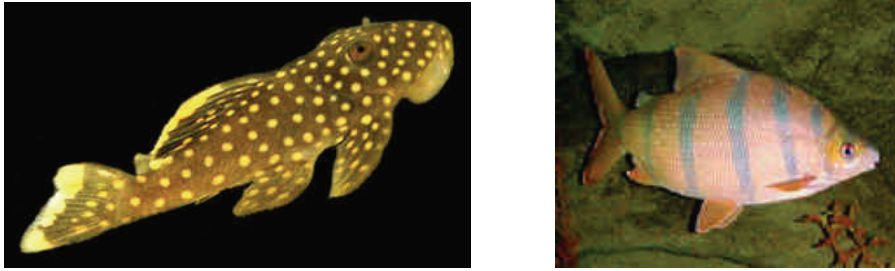


FIG. 3. Spots on Gold Nugget *Plecostomus* and stripes on *Distichodus Sexfasciatus*.

Nishiura and Ohnishi identified (1.1) as a formal singular limit of the Euler–Lagrange equation of (1.3) [12]. Ren and Wei noted that (1.1) is the  $\Gamma$ -limit of (1.3) as  $\epsilon$  tends to 0 [15] and hence put the convergence of  $I$  to its singular limit  $J$  under a rigorous mathematical framework. The lamellar phase of diblock copolymers has been studied in [5, 16, 2], the cylindrical phase in [18, 17], and the spherical phase in [19].

Another place where one finds (1.2) is the Gierer–Meinhardt theory for morphogenesis in cell development. It is a minimal model that provides a theoretical bridge between observations on the one hand and the deduction of the underlying molecular-genetic mechanisms on the other hand. Mathematically it is an activator-inhibitor type reaction-diffusion system with two unknowns of space variable  $x \in D \subset \mathbb{R}^2$  and time variable  $t > 0$ . The first unknown, denoted by  $u$ , describes the short-range autocatalytic substance, i.e., the activator, and the second unknown, denoted by  $v$ , is its long-range antagonist, i.e., the inhibitor. They satisfy the equations

$$(1.4) \quad u_t = \epsilon^2 \Delta u - u + \frac{u^p}{(1 + \kappa u^p)v^q}, \quad v_t = d \Delta v - v + \frac{u^r}{v^s}.$$

Here  $u$  and  $v$  satisfy the Neumann condition on the boundary of  $D$ , i.e.,

$$(1.5) \quad \partial_\nu u(x, t) = \partial_\nu v(x, t) = 0 \quad \forall x \in \partial D, \forall t > 0,$$

where  $\partial_\nu$  is the outward normal derivative operator on the boundary of  $D$ .

Activator-inhibitor systems were studied by Turing [21]. They may be used to model animal coats and skin pigmentation; see Figure 3. In Appendix A we give a formal justification for the convergence of steady states of (1.4) to solutions of (1.2). In this paper we study the first stage of the saturation process depicted in the second image of Figure 1. We show that when  $a$  is sufficiently small and  $\gamma$  is in a particular range, on a generic domain there exist two solutions to (1.2), each of which has the shape of a small oval set. The location and direction of each oval droplet solution are determined via the regular part  $R$  of the Green's function of the domain  $D$ . The precise definition of  $R$  is given in (2.1). Note that the regular part  $R(x, y) = R(x_1, x_2, y_1, y_2)$  is a function of two sets of variables  $x \in D$  and  $y \in D$ , each of which has two components. The diagonal of  $R$ , given by  $\tilde{R}(z) = R(z, z)$ , is a function defined on  $D$ . If  $z \rightarrow \partial D$ ,  $\tilde{R}(z) \rightarrow \infty$ . Hence  $\tilde{R}$  has at least one global minimum in  $D$ .

It is often convenient to use another parameter  $\rho$  in place of  $a$ . We set

$$(1.6) \quad \rho = \sqrt{\frac{a|D|}{\pi}}.$$

It is the average radius of a set  $E$  whose measure is fixed at  $a|D|$ . In other words if  $E$  were a round disc of the same measure  $a|D|$ ,  $\rho$  would be the radius of  $E$ . The

first stage of saturation occurs if  $\gamma$  is slightly greater than  $\frac{12}{\rho^3}$ . The number  $\frac{12}{\rho^3}$  first emerged in the proof of an existence theorem for a round droplet solution in [18]. We will explain in section 2 that it is the first point to avoid in order to have the existence of the round droplet solution, and the stability of the round droplet solution changes as  $\gamma$  moves past it.

Our first result in this paper is the following.

**OBSERVATION 1.1.** *A vector  $S \in R^2$  is determined by the domain  $D$  via the second derivatives of  $R$  at a global minimum  $\zeta$  of  $\tilde{R}$ . If  $S \neq (0, 0)$ , there exists  $\delta > 0$  such that for each  $c \in (12, 12 + \delta)$  there exists  $\rho_0 > 0$  so that (1.2) admits two oval shaped droplet solutions, both centered at  $\zeta$ , if  $\gamma = \frac{c}{\rho^3}$  and  $\rho < \rho_0$ .*

Because of the symmetry  $R(x, y) = R(y, x)$ ,  $\frac{\partial R(z, z)}{\partial x_j} = \frac{\partial R(z, z)}{\partial y_j} = \frac{1}{2} \frac{\partial \tilde{R}(z)}{\partial z_j}$ ,  $j = 1, 2$ , and consequently

$$(1.7) \quad \frac{\partial R(\zeta, \zeta)}{\partial x_1} = \frac{\partial R(\zeta, \zeta)}{\partial x_2} = 0.$$

In some sense a global minimum of  $\tilde{R}$  is a center of  $D$ . Interestingly one can define a major axis and a minor axis on a generic domain  $D$ . Let a vector  $S = (S_1, S_2)$  be given by

$$(1.8) \quad S_1 = \frac{1}{2} \left( \frac{\partial^2 R(\zeta, \zeta)}{\partial x_1^2} - \frac{\partial^2 R(\zeta, \zeta)}{\partial x_2^2} \right), \quad S_2 = \frac{\partial^2 R(\zeta, \zeta)}{\partial x_1 \partial x_2}.$$

The domain  $D$  is considered generic, or nondegenerate, with respect to  $\xi$ , if  $(S_1, S_2) \neq (0, 0)$ . In this case let  $\sigma$  be an angle such that

$$(1.9) \quad \cos 2\sigma = \frac{S_1}{|(S_1, S_2)|}, \quad \sin 2\sigma = \frac{S_2}{|(S_1, S_2)|}.$$

The minor axis is the line whose angle is  $\sigma$  and the major axis is the line whose angle is  $\sigma + \frac{\pi}{2}$ . The two oval droplets align themselves along the major and minor axes, respectively; see Figure 4.

**OBSERVATION 1.2.** *One of the two oval droplet solutions found in Observation 1.1 is stable and is parallel to the major axis whose angle is  $\sigma + \frac{\pi}{2}$ ; the other oval droplet solution is unstable and is parallel to the minor axis whose angle is  $\sigma$ .*

If  $D$  is a rectangle with its length greater than its height, we found numerically that  $S_1 < 0$  and  $S_2 = 0$ . Therefore  $\sigma = \frac{\pi}{2}$  and  $\sigma + \frac{\pi}{2} = \pi$ . So the major axis is parallel to the length side and the minor axis is parallel to the height side. The two oval droplet solutions are depicted in Figure 5.

The degenerate case  $S = (0, 0)$  is not covered in the two observations above. It occurs if for instance  $D$  is a disc or a perfect square. These two domains have no distinct major or minor axes.

Results similar to Observation 1.1 have appeared in many other problems in recent decades [7, 20, 14], etc. To our knowledge, Observation 1.2 is new. It is the first result that links the direction of a solution to the shape of the domain via the second derivatives of  $R$ .

This paper is organized as follows. Some existing results regarding round droplet solutions are recalled in section 2. In section 3, we describe the shape of an oval droplet by identifying some bifurcation solutions of a rescaled version of (1.2) formulated on the entire plane  $R^2$ . In section 4, we study (1.2) on a bounded domain  $D$  and find

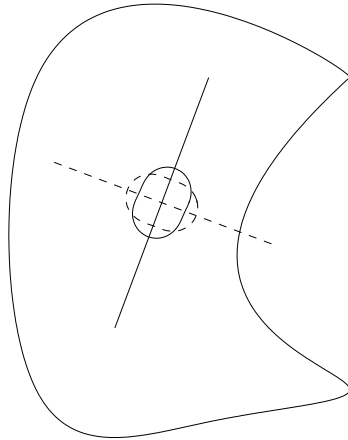


FIG. 4. The solid line and the dashed line are the major and minor axes, respectively. The stable oval droplet solution (in the solid curve) is parallel to the major axis and the unstable oval droplet solution (in the dashed curve) is parallel to the minor axis.

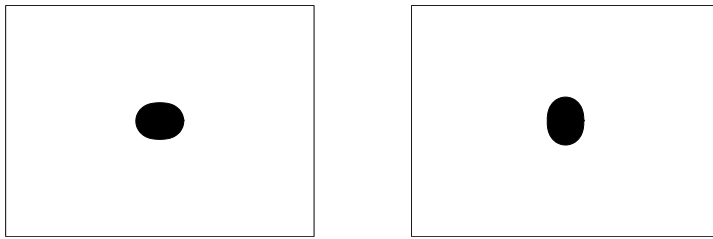


FIG. 5. The domain  $D$  is  $(0, 6) \times (0, 4)$  and  $S = (-0.0118, 0)$  found numerically. The first droplet solution is stable while the second is unstable.

two solutions with the shape of oval droplets. We also determine the location of these droplets. In section 5, we show that the direction of the oval droplets must be along either the major axis or the minor axis of the domain. A few remarks are included in section 6. The first appendix gives a formal derivation of (1.2) from the Gierer–Meinhardt system (1.4); the second appendix contains some technical calculations.

For simplicity we often write  $e^{i\theta}$  for  $(\cos \theta, \sin \theta)$ , although no complex structure is used.

**2. Round droplet solutions.** The oval droplet solutions obtained in this paper are related to an imperfect bifurcation phenomenon of round droplet solutions, so in this section we recall some existing results about these solutions. A round droplet solution on a two dimensional domain models a cross section of the cylindrical phase of diblock copolymers (see Figure 2(middle)) or the spot pattern on animal skins (see Figure 3(left)).

The Green’s function of  $-\Delta$  with the Neumann boundary condition is denoted by  $G$ . It is a sum of two parts:

$$(2.1) \quad G(x, y) = \frac{1}{2\pi} \log \frac{1}{|x - y|} + R(x, y).$$

The regular part of  $G(x, y)$  is  $R(x, y)$ . The Green's function satisfies the equation

$$-\Delta_x G(x, y) = \delta(x-y) - \frac{1}{|D|} \text{ in } D, \quad \partial_{\nu(x)} G(x, y) = 0 \text{ on } \partial D, \quad \int_D G(x, y) dx = 0 \quad \forall y \in D.$$

Here  $\Delta_x$  is the Laplacian with respect to the  $x$ -variable of  $G$ , and  $\nu(x)$  is the outward normal direction at  $x \in \partial D$ . We set

$$(2.2) \quad F(\xi_1, \xi_2, \dots, \xi_K) = \sum_{k=1}^K R(\xi_k, \xi_k) + \sum_{k=1}^K \sum_{l=1, l \neq k}^K G(\xi_k, \xi_l)$$

for  $\xi_k \in D$  and  $\xi_k \neq \xi_l$  if  $k \neq l$ . Because  $G(x, y) \rightarrow \infty$  if  $|x - y| \rightarrow 0$  and  $R(x, x) \rightarrow \infty$  if  $x \rightarrow \partial D$ ,  $F$  admits at least one global minimum.

The first result shows the existence of a solution with a pattern of round droplets.

**THEOREM 2.1** (see [17]). *Let  $K \geq 1$  be an integer and*

$$(2.3) \quad \rho = \sqrt{\frac{a|D|}{K\pi}}.$$

1. *For every  $\epsilon > 0$  there exists  $\delta > 0$ , depending on  $\epsilon, K$ , and  $D$  only, such that if*

$$(2.4) \quad \gamma\rho^3 \log \frac{1}{\rho} > 1 + \epsilon,$$

$$(2.5) \quad |\gamma\rho^3 - 2n(n+1)| > \epsilon n^2 \quad \forall n = 2, 3, 4, \dots,$$

and

$$(2.6) \quad \rho < \delta,$$

*then there exists a solution  $E$  of (1.2) which is a union of  $K$  disconnected components.*

2. *Each component is close to a round disc whose radius is  $\rho$ .*
3. *Let the centers of these discs be  $\zeta_1, \zeta_2, \dots, \zeta_K$ . Then  $\zeta = (\zeta_1, \zeta_2, \dots, \zeta_K)$  is a global minimum of the function  $F$ .*

The first condition (2.4) is an anticoarsening condition. It prevents droplets from growing or shrinking. This condition is not needed if  $K = 1$ . The second condition (2.5) is known as the resonance condition, also called the gap condition. The next theorem shows that the stability of the droplet pattern depends on how (2.5) is satisfied.

**THEOREM 2.2** (see [17]). *If (2.5) is satisfied because*

$$(2.7) \quad \gamma\rho^3 - 2n(n+1) < -\epsilon n^2 \quad \forall n \geq 2,$$

*then the round droplet solution is stable. Otherwise if (2.5) is satisfied but*

$$(2.8) \quad \epsilon n^2 < \gamma\rho^3 - 2n(n+1) \quad \text{and} \quad \gamma\rho^3 - 2(n+1)(n+2) < -\epsilon(n+1)^2$$

*for some  $n \geq 2$ , then the round droplet solution is unstable.*

The single droplet case, i.e.,  $K = 1$ , was treated in [18]. The three dimensional analogies of the two theorems were proved in [19]. Solutions there are unions of a number of small sets that are close to balls.

The first resonance point in (2.5) is relevant to the saturation phenomenon we are studying in this paper. This is the first number 12 in the sequence  $2n(n+1)$  attained when  $n = 2$ . The round droplet solution changes from being stable to unstable when  $\gamma$  increases past  $\frac{12}{\rho^3}$ . In the case when  $D$  is a unit disc and the droplet solution is a smaller concentric disc, the gap condition (2.5) is not necessary for the existence result (Theorem 2.1). This solution clearly exists for all values of  $\gamma$ . One can perform a simple bifurcation analysis and show that inside each gap there is a bifurcation point and the bifurcation diagram has the shape of a line and a paraboloid like surface. Each solution represented by a point on the surface has an oval shape.

In this paper we will show that the situation in a general domain is not so simple. If the domain does not have enough symmetry, only two oval shaped solutions can be found when  $\gamma$  is near  $\frac{12}{\rho^3}$ . The two oval sets have particular directions determined by the nonsymmetric domain. They appear as a type of imperfect bifurcation solution.

**3. The shape of an oval droplet.** The shape of an oval droplet solution is approximately determined by a solution of a problem in the entire plane  $R^2$ .

We define a free energy functional

$$(3.1) \quad J_{R^2}(E) = P_{R^2}(E) + \frac{c}{2} \int_E \Gamma(\chi_E)(x) dx.$$

The functional (3.1) is used to model an enlarged droplet, so we impose the constraint

$$(3.2) \quad |E| = \pi.$$

The parameter  $c > 0$  here is a scaled version of  $\gamma$  in (1.2). The perimeter  $P_{R^2}(E)$  of  $E$  in  $R^2$  is the length of  $\partial E$ . The operator  $\Gamma$  denotes the Newtonian potential operator given by

$$(3.3) \quad \Gamma(\chi_E)(x) = \int_{R^2} \frac{1}{2\pi} \left( \log \frac{1}{|x-y|} \right) \chi_E(y) dy.$$

The Euler–Lagrange equation of (3.1) is

$$(3.4) \quad H(\partial E) + c\Gamma(E) = \lambda \quad \text{on } \partial E,$$

where the constant  $\lambda$  is the Lagrange multiplier from the constraint  $|E| = \pi$  on  $\partial E$ .

Consider sets that can be parametrized in the polar coordinates in the following way. There is a  $2\pi$ -periodic function  $u$  such that

$$(3.5) \quad E = \bigcup_{\theta \in [0, 2\pi]} \left( \bigcup_{r \in [0, \sqrt{1+u(\theta)}]} \{re^{i\theta}\} \right).$$

The requirement that  $|E| = \pi$  implies that

$$(3.6) \quad \int_0^{2\pi} u(\theta) d\theta = 0$$

for  $|E| = \int_0^{2\pi} \int_0^{\sqrt{1+u(\theta)}} r dr d\theta = \int_0^{2\pi} \frac{1+u(\theta)}{2} d\theta = \pi$ .

Obviously the unit disc  $B(0, 1) = \{x \in R^2 : |x| < 1\}$ , corresponding to  $u = 0$ , is a solution for any  $c > 0$ . The spectrum of the linearized operator of (3.4) at the unit disc was found in [18].

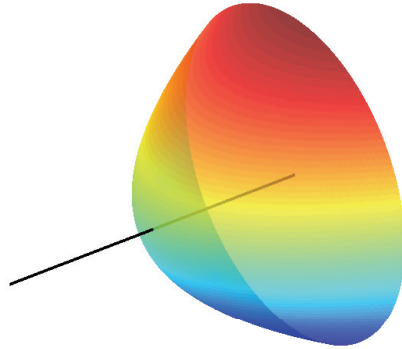


FIG. 6. The bifurcation diagram when  $c$  is near 12.

LEMMA 3.1 (see [18]). *The eigenvalues of the linearized operator at  $B(0, 1)$  are*

$$\Lambda_{c,n} = \frac{n^2 - 1}{2} + \frac{c(1 - n)}{4n}, \quad n = 1, 2, 3 \dots$$

*The corresponding eigenfunctions are  $\cos n\theta$  and  $\sin n\theta$ .*

Due to the translation invariance of this problem, one always has  $\Lambda_{c,1} = 0$  with the eigenfunctions  $\cos \theta$  and  $\sin \theta$ . We will address only stability modulo translation. The other eigenvalues,  $\Lambda_{c,2}, \Lambda_{c,3}, \Lambda_{c,4}, \dots$ , are all positive if  $0 < c < 12$ ; when  $c = 12$ ,  $\Lambda_{12,2} = 0$ . In general if  $c = 2n(n + 1)$ , where  $n = 2, 3, 4 \dots$ , then  $\Lambda_{2n(n+1),n} = 0$ .

It is not too hard to see that all these  $2n(n + 1)$ ,  $n = 2, 3, 4 \dots$ , are bifurcation points. Let us treat the  $n = 2$  case. The other cases can be dealt with in a similar way. When  $c = 2n(n + 2) = 12$ ,  $\Lambda_{12,2} = 0$ . The eigenfunctions of  $\Lambda_{12,2}$  are  $\cos 2\theta$  and  $\sin 2\theta$ , both of which are  $\pi$ -periodic. We look for bifurcation solutions among  $\pi$ -periodic  $u$ 's of zero average. Such  $u$ 's are expanded as

$$(3.7) \quad u(\theta) = \sum_{j=1}^{\infty} (A_{2j} \cos 2j\theta + B_{2j} \sin 2j\theta).$$

It can be shown that the bifurcation diagram is of the generalized pitch-fork type; see Figure 6. The diagram consists of a line and a surface that is similar to a paraboloid. The line represents the trivial solution  $u = 0$  and the surface represents the bifurcation solutions. Whether the bifurcation solutions are stable depends on whether the paraboloid opens toward the larger  $c$  direction (the supercritical case) or the smaller  $c$  direction (the subcritical case). Numerical calculations suggest that it is the supercritical case. We make the following assumption in this paper.

HYPOTHESIS 3.2. *The bifurcation diagram at  $c = 12$  is supercritical. Hence the bifurcation solutions of (3.4) at  $c = 12$  are stable.*

Following Hypothesis 3.2 we have  $\delta > 0$  such that for each

$$(3.8) \quad c \in (12, 12 + \delta)$$

there exists a family of bifurcation solutions. Among this family one solution, which we denote by  $\tilde{u}$ , satisfies

$$(3.9) \quad A_2 > 0 \quad \text{and} \quad B_2 = 0,$$

where  $A_2$  and  $B_2$  are the coefficients of  $\cos 2\theta$  and  $\sin 2\theta$ , respectively, in the expansion (3.7) of  $\tilde{u}$ . Then  $\tilde{u}$  has the form

$$(3.10) \quad \tilde{u} = d \cos 2\theta + \tilde{u}^\perp(\cdot, c, d),$$

where  $d > 0$  and  $\tilde{u}^\perp$  is of order  $d^2$ . We have denoted the  $A_2$  coefficient of  $\tilde{u}$  by  $d$ . Other bifurcation solutions, with the same  $c$  value, are obtained from  $\tilde{u}$  by a rotation of angle  $\Omega$ . We denote them by

$$(3.11) \quad u(\theta, \Omega) = \tilde{u}(\theta - \Omega).$$

Each solution  $u(\cdot, \Omega)$  of (3.4) is degenerate since the linearized operator has a three dimensional kernel at  $u$ . The kernel is spanned by  $T_1, T_2$ , and  $P$ , where

$$(3.12) \quad T_1(\theta, \Omega) = \sqrt{1 + u(\theta, \Omega)} \cos(\theta - \Omega), \quad T_2(\theta, \Omega) = \sqrt{1 + u(\theta, \Omega)} \sin(\theta - \Omega), \quad P(\theta, \Omega) = \frac{\partial u(\theta, \Omega)}{\partial \Omega}.$$

Geometrically  $T_1$  and  $T_2$  come from the translation invariance of the problem and  $P$  comes from the rotation invariance. More specifically place  $u(\cdot, \Omega)$  in (3.4) and differentiate the equation with respect to  $\Omega$ . Then  $P$  appears as a member in the kernel.

To see  $T_1$  and  $T_2$  are also in the kernel, consider the solution  $\tilde{u}$ . Let us shift the set  $E_{\tilde{u}}$  determined by the function  $\tilde{u}$  along the horizontal axis by  $h \in R$ . Denote the new set by  $E^h = \{x \in R^2 : x - (h, 0) \in E_{\tilde{u}}\}$ . Let the boundary of  $E_h$  be parametrized by  $v(\eta), \eta \in [0, 2\pi]$ , where  $v(\eta)$  is  $2\pi$ -periodic and is related to  $\tilde{u}(\theta)$  via

$$(3.13) \quad \sqrt{1 + v(\eta)} e^{i\eta} = (h, 0) + \sqrt{1 + \tilde{u}(\theta)} e^{i\theta}.$$

Inserting  $v$  into (3.4) and differentiating the equation with respect to  $h$  yields that  $\frac{\partial v}{\partial h}|_{h=0}$  is in the kernel of the linearized operator. Implicit differentiation of (3.13) shows that

$$\begin{aligned} \begin{bmatrix} \frac{\partial \eta}{\partial \theta} & \frac{\partial \eta}{\partial h} \\ \frac{\partial v}{\partial \theta} & \frac{\partial v}{\partial h} \end{bmatrix} &= - \begin{bmatrix} \sqrt{1 + v} \sin \eta & -\frac{\cos \eta}{2\sqrt{1+v}} \\ -\sqrt{1 + v} \cos \eta & -\frac{\sin \eta}{2\sqrt{1+v}} \end{bmatrix}^{-1} \begin{bmatrix} \frac{\cos \theta}{2\sqrt{1+\tilde{u}}} \frac{\partial \tilde{u}}{\partial \theta} - \sqrt{1 + \tilde{u}} \sin \theta & 1 \\ \frac{\sin \theta}{2\sqrt{1+\tilde{u}}} \frac{\partial \tilde{u}}{\partial \theta} + \sqrt{1 + \tilde{u}} \cos \theta & 0 \end{bmatrix} \\ &= \begin{bmatrix} \frac{-\sin \eta}{\sqrt{1+v}} & \frac{\cos \eta}{\sqrt{1+v}} \\ 2\sqrt{1 + v} \cos \eta & 2\sqrt{1 + v} \sin \eta \end{bmatrix} \begin{bmatrix} \frac{\cos \theta}{2\sqrt{1+\tilde{u}}} \frac{\partial \tilde{u}}{\partial \theta} - \sqrt{1 + \tilde{u}} \sin \theta & 1 \\ \frac{\sin \theta}{2\sqrt{1+\tilde{u}}} \frac{\partial \tilde{u}}{\partial \theta} + \sqrt{1 + \tilde{u}} \cos \theta & 0 \end{bmatrix}. \end{aligned}$$

This implies that

$$(3.14) \quad \frac{\partial v}{\partial h} \Big|_{h=0} = 2\sqrt{1 + v(\eta)} \cos \eta \Big|_{h=0} = 2\sqrt{1 + \tilde{u}(\theta)} \cos \theta.$$

Therefore  $\sqrt{1 + \tilde{u}(\theta)} \cos \theta$  is in the kernel of the linearized operator at  $\tilde{u}$ . A similar argument with a shift of  $E_{\tilde{u}}$  along the vertical direction shows that  $\sqrt{1 + \tilde{u}(\theta)} \sin \theta$  is also in the kernel. Finally a rotation by an angle  $\Omega$  shows that  $T_1$  and  $T_2$  are in the kernel of the linearized operator at  $u(\cdot, \Omega)$ .

It follows from the fact that  $\tilde{u}$  has no  $\sin 2\theta$  component that  $T_1$  and  $T_2$  are orthogonal. Since the integral of any  $\pi$ -periodic function multiplied by  $\cos \theta$  or  $\sin \theta$  is zero,  $T_j$  and  $P$  are orthogonal. Hence  $T_1, T_2$ , and  $P$  form an orthogonal basis. Moreover  $T_1, T_2$ , and  $P$  are all perpendicular to 1.

**4. The location of an oval droplet.** From now on we consider (1.2) on a bounded domain  $D$  with a small  $a$ . The profile determined by  $u(\theta, \Omega)$  will be scaled down to become an approximate solution. We set

$$(4.1) \quad \gamma = \frac{c}{\rho^3}.$$

The constant  $c$  is fixed in the range  $(12, 12 + \delta)$  determined in (3.8), and  $\rho$  is sufficiently small. As claimed in Observations 1.1 and 1.2, under Hypothesis 3.2 two oval shaped, droplet solutions will be found. One is stable and the other one is unstable.

If Hypothesis 3.2 were false, one could still find two oval droplet solutions, this time for  $c \in (12 - \delta, 12)$ . However, if this were to occur, the bifurcation diagram of (3.4) near  $c = 12$  would be subcritical. Consequently the two oval droplet solutions found on a bounded domain would both be unstable.

Given a subset  $E$  of  $D$  whose measure is fixed at  $|E| = a|D| = \pi\rho^2$ , in addition to the operators  $H$  and  $\Gamma$  given in section 3, we define another operator  $R$  by

$$(4.2) \quad R(E)(x) = \int_E R(x, y) dy,$$

where  $R(x, y)$  is the regular part of the Green's function  $G$  (see (2.1)).

Let  $\xi \in D$  be an arbitrary point and  $w(\theta, \Omega) = \rho^2 u(\theta, \Omega)$ . Define a set  $E_w$  by

$$(4.3) \quad E_w = \bigcup_{\theta \in [0, 2\pi]} \left( \bigcup_{r \in [0, \sqrt{\rho^2 + w(\theta)}]} \{\xi + r e^{i\theta}\} \right).$$

$E_w$  is a scaled down version of  $E_u$ , centered at  $\xi$ . Note that  $|E_w| = \pi\rho^2 = a|D|$ . This set serves as an approximate solution. To find an exact solution, we perturb  $w$  by another zero average function  $\phi$  to  $w + \phi$ . When acting on  $E_{w+\phi}$ , the operators  $H$ ,  $\Gamma$ , and  $R$  are considered as operators on the function  $w + \phi$ . Then  $w + \phi$  satisfies

$$(4.4) \quad H(w + \phi) + \gamma(\Gamma(w + \phi) + R(w + \phi)) = Const.$$

Equation (4.4) holds on the boundary of  $E_{w+\phi}$ . Since the boundary is parametrized by  $\theta$ ,  $H(w + \phi)$ ,  $\Gamma(w + \phi)$ , and  $R(w + \phi)$  are all functions of  $\theta$ . Linearizing (4.4) and using the fact that  $H(w) + \gamma\Gamma(w) = Const.$ , we find that  $\phi$  approximately satisfies

$$(4.5) \quad [H'(w) + \gamma\Gamma'(w)]\phi + \gamma R(w) \approx Const.$$

The linearized operator  $H'(w) + \gamma\Gamma'(w)$  is self-adjoint and has the kernel spanned by  $T_1$ ,  $T_2$ , and  $P$ . Three solvability conditions follow:

$$(4.6) \quad R(w) \perp T_j \quad (j = 1, 2) \quad \text{and} \quad R(w) \perp P.$$

We use them to determine  $\xi$  and  $\Omega$ .

To this end we expand  $R(w)$  in terms of  $\rho$ :  $R(w) = \sum_{k=0}^{\infty} \frac{\rho^k}{k!} \frac{\partial^k R}{\partial \rho^k} \Big|_{\rho=0}$ . Calculations in Appendix B show that

$$R|_{\rho=0} = 0, \quad \frac{\partial R}{\partial \rho} \Big|_{\rho=0} = 0, \quad \text{and} \quad \frac{\partial^2 R}{\partial \rho^2} \Big|_{\rho=0} = 2\pi R(\xi, \xi).$$

Here  $2\pi R(\xi, \xi)$  is a constant independent of  $\theta$ . The first three terms in the expansion of  $R(w)$  are all perpendicular to  $T_j$  and  $P$ , and no information can be deduced from them. The next order is

$$\frac{\partial^3 R}{\partial \rho^3} \Big|_{\rho=0} = 6\pi R_x(\xi, \xi) [\sqrt{1 + u(\theta)} e^{i\theta}].$$

We use  $R_x(\xi, \xi)$  to denote the vector  $(\frac{\partial R}{\partial x_1}, \frac{\partial R}{\partial x_2})$  of the two partial derivatives at the point  $(\xi, \xi)$ . The quantity  $R_x(\xi, \xi)[\sqrt{1+ue^{i\theta}}]$  is just the inner product of  $R_x(\xi, \xi)$  and  $\sqrt{1+ue^{i\theta}}$ . For a more consistent notation we view  $R_x(\xi, \xi)$  as a linear functional and view the inner product as the result of the functional on the vector  $\sqrt{1+ue^{i\theta}}$ . We also need to expand  $\xi$  in terms of  $\rho$  so that

$$(4.7) \quad \xi = \zeta + \rho\eta + \dots,$$

where  $\zeta$  and  $\eta$  are independent of  $\rho$ . Then

$$(4.8) \quad \frac{\partial^3 R}{\partial \rho^3} \Big|_{\rho=0} = 6\pi R_x[\sqrt{1+ue^{i\theta}}] + \rho 6\pi R_{xx}[\eta, \sqrt{1+ue^{i\theta}}] + \rho 6\pi R_{xy}[\sqrt{1+ue^{i\theta}}, \eta] + O(\rho^2).$$

We have used the shorthand notation

$$(4.9) \quad R_x = \left( \frac{\partial R(\zeta, \zeta)}{\partial x_1}, \frac{\partial R(\zeta, \zeta)}{\partial x_2} \right)$$

for the vector and

$$(4.10) \quad R_{xx} = \begin{bmatrix} \frac{\partial^2 R(\zeta, \zeta)}{\partial x_1^2} & \frac{\partial^2 R(\zeta, \zeta)}{\partial x_1 \partial x_2} \\ \frac{\partial^2 R(\zeta, \zeta)}{\partial x_2 \partial x_1} & \frac{\partial^2 R(\zeta, \zeta)}{\partial x_2^2} \end{bmatrix}, \quad R_{xy} = \begin{bmatrix} \frac{\partial^2 R(\zeta, \zeta)}{\partial x_1 \partial y_1} & \frac{\partial^2 R(\zeta, \zeta)}{\partial x_1 \partial y_2} \\ \frac{\partial^2 R(\zeta, \zeta)}{\partial x_2 \partial y_1} & \frac{\partial^2 R(\zeta, \zeta)}{\partial x_2 \partial y_2} \end{bmatrix}$$

for the matrices.  $R_{xx}[\eta, \sqrt{1+ue^{i\theta}}]$  is the result of the matrix  $R_{xx}$ , considered as a bilinear form, acting on the vectors  $\eta$  and  $\sqrt{1+ue^{i\theta}}$ , and  $R_{xy}[\sqrt{1+ue^{i\theta}}, \eta]$  is the result of the matrix  $R_{xy}$  acting on  $\sqrt{1+ue^{i\theta}}$  and  $\eta$ .

Hence the  $\rho^3$  order of  $R(w)$  is

$$(4.11) \quad \frac{6\pi\rho^3}{3!} R_x[\sqrt{1+ue^{i\theta}}].$$

Now examine the  $\rho^3$  order terms in  $\langle R(w), T_j \rangle = 0$  ( $j = 1, 2$ ) and  $\langle R(w), P \rangle = 0$ . The last equation implies that

$$(4.12) \quad \left\langle R_x[\sqrt{1+ue^{i\theta}}], \frac{\partial u}{\partial \Omega} \right\rangle = 0,$$

which always holds since  $\sqrt{1+ue^{i\theta}} \frac{\partial u}{\partial \Omega}$  is  $\pi$ -periodic, and the integral of any  $\pi$ -periodic function multiplied by  $e^{i\theta}$  is 0.

The equation  $\langle R_x[\sqrt{1+ue^{i\theta}}], T_1 \rangle = 0$  implies that

$$\int_0^{2\pi} (1+u)(R_{x_1}(\zeta, \zeta) \cos \theta + R_{x_2}(\zeta, \zeta) \sin \theta) \cos(\theta - \Omega) d\theta = 0.$$

Note that

$$\begin{aligned} \int_0^{2\pi} (1+u) \cos \theta \cos(\theta - \Omega) d\theta &= \int_0^{2\pi} (1+u)[\cos(\theta - \Omega) \cos \Omega - \sin(\theta - \Omega) \sin \Omega] \cos(\theta - \Omega) \\ &= \cos \Omega \|T_1\|_2^2 - \frac{\sin \Omega}{2} \langle 1+u, \sin 2(\theta - \Omega) \rangle = \cos \Omega \|T_1\|_2^2, \end{aligned}$$

where the last step follows from the fact that  $\tilde{u}(\theta)$  has no  $\sin 2\theta$  component. Similarly

$$(4.13) \quad \int_0^{2\pi} (1+u) \sin \theta \cos(\theta - \Omega) d\theta = \sin \Omega \|T_1\|_2^2.$$

We therefore obtain the consequence that

$$(4.14) \quad R_{x_1}(\zeta, \zeta) \cos \Omega + R_{x_2}(\zeta, \zeta) \sin \Omega = 0.$$

In a similar way the equation  $\langle R(w), T_2 \rangle = 0$  implies that

$$(4.15) \quad -R_{x_1}(\zeta, \zeta) \sin \Omega + R_{x_2}(\zeta, \zeta) \cos \Omega = 0.$$

Equations (4.14) and (4.15) form a nonsingular linear homogeneous system, so

$$(4.16) \quad R_{x_1}(\zeta, \zeta) = R_{x_2}(\zeta, \zeta) = 0.$$

Because of the symmetry  $R(x, y) = R(y, x)$ , (4.16) means that  $\zeta$  is a critical point of the diagonal  $\tilde{R}(z) = R(z, z)$ . Since  $\tilde{R}(z) \rightarrow \infty$  as  $z \rightarrow \partial D$ , the global minimum of  $\tilde{R}$  is attained in  $D$ . One can have  $\zeta$  in (4.16) to be this minimum of  $\tilde{R}$ . This completes our justification of Observation 1.1.

**5. The direction of an oval droplet.** Calculations in Appendix B show that

$$(5.1) \quad \left. \frac{\partial^4 R}{\partial \rho^4} \right|_{\rho=0} = 12\pi R_{xx}(\xi, \xi)[\sqrt{1+ue^{i\theta}}, \sqrt{1+ue^{i\theta}}] + Const.$$

Because of (4.8) the  $\rho^4$  order of  $R(w)$  is

$$(5.2) \quad \begin{aligned} & \frac{24\pi\rho^4}{4!}R_{xx}[\eta, \sqrt{1+ue^{i\theta}}] + \frac{24\pi\rho^4}{4!}R_{xy}[\sqrt{1+ue^{i\theta}}, \eta] \\ & + \frac{12\pi\rho^4}{4!}R_{xx}[\sqrt{1+ue^{i\theta}}, \sqrt{1+ue^{i\theta}}] + Const. \end{aligned}$$

In the  $\rho^4$  order of  $\langle R(w), P \rangle$ , since  $P$  is  $\pi$ -periodic, the inner products of  $P$  with the first two terms in (5.2) are 0. Hence we have

$$(5.3) \quad \langle R_{xx}[\sqrt{1+ue^{i\theta}}, \sqrt{1+ue^{i\theta}}], P \rangle = 0.$$

Let us set  $S_1$  and  $S_2$  by (1.8) and introduce  $\sigma \in [0, 2\pi)$  so that

$$(5.4) \quad \cos 2\sigma = \frac{S_1}{\sqrt{S_1^2 + S_2^2}}, \quad \sin 2\sigma = \frac{S_2}{\sqrt{S_1^2 + S_2^2}}.$$

Note that

$$\begin{aligned} R_{xx}[e^{i\theta}, e^{i\theta}] &= R_{x_1x_1}(\zeta, \zeta) \cos^2 \theta + 2R_{x_1x_2}(\zeta, \zeta) \cos \theta \sin \theta + R_{x_2x_2}(\zeta, \zeta) \sin^2 \theta \\ &= \sqrt{S_1^2 + S_2^2} \cos 2(\theta - \sigma) + \frac{R_{x_1x_1} + R_{x_2x_2}}{2}. \end{aligned}$$

We claim that

$$(5.5) \quad \left\langle (1+u) \frac{R_{x_1x_1} + R_{x_2x_2}}{2}, P \right\rangle = 0.$$

This is because

$$\langle 1+u, P \rangle = \langle 1 + \tilde{u}(\theta - \Omega), -\tilde{u}'(\theta - \Omega) \rangle = - \int_0^{2\pi} (1 + \tilde{u}(\theta)) \tilde{u}'(\theta) d\theta = \left( \tilde{u} + \frac{\tilde{u}^2}{2} \right) \Big|_0^{2\pi} = 0.$$

Therefore (5.3) becomes

$$\langle (1 + u) \cos 2(\theta - \sigma), P \rangle = 0, \text{ i.e., } \langle (1 + \tilde{u}(\theta - \Omega)) \cos 2(\theta - \sigma), -\tilde{u}'(\theta - \Omega) \rangle = 0.$$

A change of variable turns this to

$$(5.6) \quad - \int_0^{2\pi} (1 + \tilde{u}(\theta)) \tilde{u}'(\theta) \cos 2(\theta + \Omega - \sigma) d\theta = 0.$$

This equation determines  $\Omega$  in terms of  $\sigma$ .

Finally we consider the inner products of (5.2) with  $T_j$ . The inner products of the third term in (5.2) and  $T_j$  are 0. We deduce that

$$(5.7) \quad \langle R_{xx}[\eta, \sqrt{1 + ue^{i\theta}}] + R_{xy}[\sqrt{1 + ue^{i\theta}}, \eta], T_j \rangle = 0.$$

Arguing as in the last section we find that

$$(5.8) \quad (R_{x_1x_1} + R_{x_1y_1})\eta_1 + (R_{x_2x_1} + R_{x_1y_2})\eta_2 = 0, \quad (R_{x_1x_2} + R_{x_2y_1})\eta_1 + (R_{x_2x_2} + R_{x_2y_2})\eta_2 = 0.$$

By the the symmetry of  $R$  we deduce that

$$\begin{aligned} \frac{1}{2} \frac{\partial^2 \tilde{R}(\zeta)}{\partial z_1^2} &= R_{x_1x_1} + R_{x_1y_1}, & \frac{1}{2} \frac{\partial^2 \tilde{R}(\zeta)}{\partial z_1 \partial z_2} &= R_{x_2x_1} + R_{x_1y_2} = R_{x_1x_2} + R_{x_2y_1}, \\ \frac{1}{2} \frac{\partial^2 \tilde{R}(\zeta)}{\partial z_2^2} &= R_{x_2x_2} + R_{x_2y_2}. \end{aligned}$$

If  $\zeta$  is a nondegenerate minimum of  $\tilde{R}$ , the linear system (5.8) is nonsingular and

$$(5.9) \quad \eta = 0.$$

Recall  $\gamma = \frac{c}{\rho^3}$ . When  $c$  is close to 12, (5.6) can be solved explicitly. In this case  $\tilde{u}(\theta)$  is close to  $d \cos 2\theta$ , where  $d$  is a small positive constant and  $\tilde{u}'(\theta)$  is close to  $-2d \sin 2\theta$ . We can approximately write (5.6) as

$$(5.10) \quad 2d \int_0^{2\pi} \sin 2\theta \cos 2(\theta + \Omega - \sigma) d\theta = 0.$$

This implies that  $\Omega = \sigma + \frac{n\pi}{2}$ ,  $n = 0, 1, 2, \dots$ . We have actually found two, not four, solutions. The first one corresponds to  $\Omega = \sigma$  and the second one corresponds to  $\Omega = \sigma + \frac{\pi}{2}$ . Since  $\tilde{u}$  is  $\pi$ -periodic, we have the fact that

$$w(\cdot, \Omega) + \phi(\cdot, \Omega) = w(\cdot, \Omega + \pi) + \phi(\cdot, \Omega + \pi).$$

Therefore  $\Omega = \sigma$  and  $\Omega = \sigma + \pi$  represent the same solution; and  $\Omega = \sigma + \frac{\pi}{2}$  and  $\Omega = \sigma + \frac{3\pi}{2}$  also represent the same solution.

To determine the stability of the two solutions we study the dependence of the energy of  $w + \phi$  on  $\Omega$ . This energy of  $w + \phi$  is close to the energy of  $w$ , and it suffices to consider

$$(5.11) \quad J(w) = P_D(\partial E_w) + \frac{\gamma}{2} \int_{E_w} \int_{E_w} \frac{1}{2\pi} \log \frac{1}{|x - y|} dx dy + \frac{\gamma}{2} \int_{E_w} \int_{E_w} R(x, y) dx dy,$$

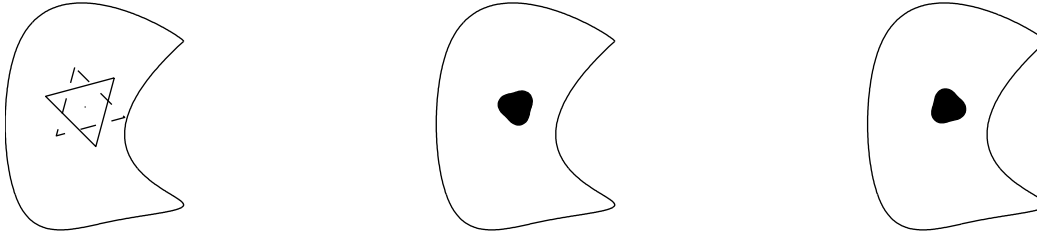


FIG. 7. (Left): The major triangle (solid line) and the minor triangle (dashed line) for a general domain. (Middle) and (right): Two triangular droplet solutions corresponding to the two triangles.

in which only the third term depends on  $\Omega$ . Hence we study the derivative of this term with respect to  $\Omega$ :

$$(5.12) \quad \frac{\partial J(w)}{\partial \Omega} = \frac{\gamma}{2} \frac{\partial}{\partial \Omega} \int_{E_w} \int_{E_w} R(x, y) \, dx dy = \frac{\gamma}{2} \int_0^{2\pi} R(w) \frac{\partial w}{\partial \Omega} \, d\theta.$$

The calculations of  $R(w)$  and  $\langle R(w), P \rangle$  earlier show that

$$(5.13) \quad \frac{\partial J(w)}{\partial \Omega} = \frac{\gamma \rho^2}{2} \int_0^{2\pi} R(w) \frac{\partial u}{\partial \Omega} \, d\theta = \frac{\gamma \rho^2}{2} \frac{\rho^4 \pi}{2} \int_0^{2\pi} -(1 + \tilde{u}(\theta)) \tilde{u}'(\theta) \cos 2(\theta + \Omega - \sigma) \, d\theta + O(\gamma \rho^7).$$

When  $c$  is close to 12, the above is approximated by

$$(5.14) \quad \frac{\partial J(w)}{\partial \Omega} \approx \frac{\gamma \rho^6 \pi}{4} \int_0^{2\pi} 2d \sin 2\theta \cos 2(\theta + \Omega - \sigma) \, d\theta = \frac{\gamma \rho^6 \pi^2}{2} (-d) \sin 2(\Omega - \sigma).$$

Note that  $d > 0$ . Hence the solution corresponding to  $\Omega = \sigma$  gives a maximum of  $J$  with respect to  $\Omega$  and therefore is unstable; the solution corresponding to  $\Omega = \sigma + \frac{\pi}{2}$  gives a minimum of  $J$  with respect to  $\Omega$  and therefore is stable.

**6. Discussion.** If Hypothesis 3.2 can be confirmed, then using a type of Lyapunov–Schmidt reduction procedure we can prove Observations 1.1 and 1.2 rigorously. If Hypothesis 3.2 is false, we can still prove Observations 1.1 and 1.2 for  $c$  in the range  $(12 - \delta, 12)$ , although the two oval droplet solutions are both unstable.

We have considered only the first resonance point  $c = 12$  corresponding to  $n = 2$ . One can also study higher resonance points  $c = 2n(n + 1)$  for  $n = 3, 4, \dots$ . The solutions found near those resonance points are all unstable. Nevertheless these solutions are quite interesting.

Consider the  $n = 3$  case first. The shape of a noncircular, droplet solution for  $\gamma$  close to  $\frac{2n(n+1)}{\rho^3} = \frac{24}{\rho^3}$  looks like a triangle with corners smoothed out. As in section 3, if we denote the profile by  $\tilde{u}$ , then  $\tilde{u}(\theta) \approx d \cos 3\theta$ . Instead of axes one can define two triangles on a generic domain  $D$  with the help of the third order derivatives of  $R$ . One of them can be termed the major triangle and the other the minor triangle. A rotation by  $\frac{\pi}{3}$  turns one triangle to the other; see Figure 7(left). There should be two triangular droplet solutions on a generic  $D$ . One is in the direction of the major triangle of  $D$  and the other is in the direction of the minor triangle of  $D$ ; see Figures 7(middle) and (right).

For a general  $n$ , when  $\gamma$  is close to  $\frac{2n(n+1)}{\rho^3}$ , there should be two  $n$ -polygon shaped (with smoothed corners) droplet solutions on a generic  $D$ . The profile is given by

$\tilde{u}(\theta) \approx d \cos n\theta$ . The  $n$ th order derivatives of  $R$  define two  $n$ -polygons for  $D$ . The two  $n$ -polygon droplets are parallel to the two  $n$ -polygons of  $D$ , respectively.

The existence of a stable oval droplet solution and an unstable oval droplet solution indicates a type of imperfect bifurcation near the first resonance point  $\frac{12}{\rho^3}$ . However, to understand the imperfect bifurcation diagram completely near  $\frac{12}{\rho^3}$ , one must consider (1.2) with a small  $\rho$  for all  $c$  near 12. This is a harder problem than the one studied in this paper, since in Observation 1.1 the number  $\rho_0$  in the restriction  $\rho < \rho_0$  depends on  $c \in (12, 12 + \delta)$ . One will have to derive results for  $\rho < \rho_0$  that hold uniformly with respect to  $c$  in a neighborhood of 12.

This paper addresses only the first stage of saturation, namely the deformation to an elongated shape from a round shape. A complete saturation theory will contain at least two more stages of transformation: appearance of necked droplets and breaking off of necked droplets. On the other hand, the opposite of saturation is simpler and much better understood. The Lifshitz–Slyozov–Wagner theory [9, 22] for the Ostwald ripening phenomenon describes how in a pattern of many droplets, some droplets grow larger while others shrink and disappear. This theory has been formulated mathematically by Niethammer [10] and Niethammer and Otto [11].

Kolokolnikov, Ward, and Wei [8] have shown that oval shaped droplets appear as time dependent solutions in dynamic problems. The shape of a dynamic oval is similar to the one discussed here. However, the oval direction there is not determined by the domain geometry. Instead it is related to the motion of the oval.

**Appendix A. The reduction of the Gierer–Meinhardt system.** In this section we derive a singular limit for (1.4). Our argument is formal. It seems possible that one may carry out a rigorous deduction using techniques developed by Del Pino, Kowalczyk, and Wei [4, 3].

The diffusion coefficient  $\epsilon^2$  of the variable  $u$  must be small:  $0 < \epsilon \ll 1$ . The diffusion coefficient of  $v$  must be large in the sense that  $d = \frac{d_0}{\epsilon}$ , where  $d_0 > 0$  is independent of  $\epsilon$ . Saturation in this problem is controlled by  $d_0$ . The smaller  $d_0$  is, the finer the pattern becomes. Moreover in the second equation of (1.4) we take  $\iota = 0$ . This case is known as the fast inhibitor limit.

The nonlinearity in the first equation of (1.4) is denoted by

$$(A.1) \quad f(u, v) = -u + \frac{u^p}{(1 + \kappa u^p)v^q}.$$

It has a cubic shape with respect to  $u$ . For each  $v > 0$ , there exist three zeros of  $f(u, v)$  as a function of  $u$ . There is a particular value  $v_0$  such that at  $v = v_0$ ,  $f(\cdot, v_0)$  becomes a balanced cubic nonlinearity, in the sense that  $\int_0^z f(u, v_0) du = 0$ . Here  $z$  is the largest zero of  $f(\cdot, v_0)$ .

We expect the  $u$  variable to develop a pattern shortly after the system (1.4) is started. A subset  $E$  of  $D$  emerges so that  $u(x, t)$  is close to  $z$  in the set  $E$  and close to 0 in the set  $D \setminus E$ . The boundary of  $E$  in  $D$  is a collection of curves which we denote by  $\Gamma$ . The value of  $u$  changes abruptly across  $\Gamma$ .

The boundary  $\Gamma$  changes in time and we denote it by  $\Gamma(\tau)$ , where  $\tau$  is a slow time variable so that  $\tau = \epsilon^2 t$ . Away from  $\Gamma(\tau)$  we take  $u \approx z\chi_E$ , where  $\chi_E$  is the characteristic function of  $E$ . The shape of  $u$  near  $\Gamma(\tau)$  is more complicated. Let  $Q(\xi, s)$  be the traveling wave solution of the problem

$$(A.2) \quad Q_{\xi\xi} + c(s)Q_{\xi} + f(Q, s) = 0, \quad \xi \in (-\infty, \infty).$$

In (A.2),  $s$  is a parameter. As  $\xi$  tends to  $-\infty$ , we require that  $Q(\xi, s)$  tend to 0, and as  $\xi$  tends to  $\infty$ , we require that  $Q(\xi, s)$  tend to the largest zero of  $f(\cdot, s)$ . The constant  $c(s)$  is the velocity of the traveling wave. It is unknown and must be determined from (A.2).

Let  $d(x, \tau)$  be the signed distance function from a point  $x$  to  $\Gamma(\tau)$ . The sign of  $d(x, \tau)$  is positive if  $x$  is in the set  $E$  and negative if  $x$  is in  $D \setminus E$ . We assume that approximately

$$(A.3) \quad u(x, t) \approx Q\left(\frac{d(x, \epsilon^2 t)}{\epsilon}, s\right),$$

where  $s$  is constant, discussed later. Insert this  $Q$  into the first equation in (1.4) to find

$$\epsilon Q_\xi d_\tau = Q_{\xi\xi} |\nabla d|^2 + \epsilon Q_\xi \Delta d + f(Q, s).$$

It is known that on the set  $\Gamma(\tau)$ ,  $|\nabla d| = 1$  and  $\Delta d(x, \tau) = H(x, \tau)$ , where  $H(x, \tau)$  is the curvature of  $\Gamma(\tau)$  at  $x$ , viewed from  $E$ . Therefore we obtain

$$(A.4) \quad Q_{\xi\xi} + (\epsilon H - \epsilon d_\tau) Q_\xi + f(Q, s) = 0.$$

Comparing (A.4) to (A.2) we deduce

$$(A.5) \quad c(s) = \epsilon H - \epsilon d_\tau.$$

Note that  $d_\tau$  is the normal velocity of the boundary  $\Gamma(\tau)$  at the slow time  $\tau$ , which we denote by  $V(\tau)$ :  $V(\tau) = d_\tau$ .

Now we discuss  $c(s)$ . On the boundary  $\Gamma(\epsilon^2 t)$ ,  $s$  must be equal to  $v(x, t)$ . However, unlike  $u(x, t)$ ,  $v(x, t)$  changes slowly in  $x$ . Asymptotically we have the expansion  $v(x, t) \approx v_0 + \epsilon w(x, t)$ , so that  $c(s) = c(v) \approx c(v_0) + \epsilon c'(v_0)w$ . Since  $v_0$  is the point where  $f(\cdot, v_0)$  is balanced,  $c(v_0) = 0$ . Hence (A.5) implies that

$$(A.6) \quad V = H - c'(v_0)w.$$

It remains to find an equation for  $w$ . In the second equation in (1.4) (with  $\iota = 0$ ) we deduce

$$\frac{d_0}{\epsilon} \Delta(v_0 + \epsilon w(x, t)) - (v_0 + \epsilon w(x, t)) + \frac{u^r}{(v_0 + \epsilon w(x, t))^s} = 0.$$

As  $\epsilon \rightarrow 0$ , we find

$$(A.7) \quad d_0 \Delta w - v_0 + \frac{z^r}{v_0^s} \chi_E = 0.$$

Equations (A.6) and (A.7) form a system for the evolution of the boundary  $\Gamma$ :

$$(A.8) \quad V = H - c'(0)w \text{ on } \Gamma, \quad d_0 \Delta w - v_0 + \frac{z^r}{v_0^s} \chi_E = 0 \text{ in } D.$$

Note that the Neumann boundary condition for  $v$  implies the same boundary condition for  $w$  and hence

$$\int_D \left(-v_0 + \frac{z^r}{v_0^s} \chi_E\right) dx = 0.$$

Therefore  $|E| = \frac{v_0^{s+1}}{z^r} |D|$ . Define

$$(A.9) \quad a = \frac{v_0^{s+1}}{z^r}, \quad \gamma = -\frac{c'(v_0)z^r}{d_0 v_0^s}.$$

A steady state satisfies  $V = 0$ . Then (A.8) becomes (1.2).

**Appendix B. Expansion of  $R(w)$ .** Recall that

$$\begin{aligned} R(w)(\theta) &= \int_{E_w} R(\xi + \rho\sqrt{1+ue^{i\theta}}, y) dy \\ &= \int_0^{2\pi} \int_0^{\rho\sqrt{1+u(\omega)}} R(\xi + \rho\sqrt{1+u(\theta)}e^{i\theta}, \xi + te^{i\omega}) t dt d\omega. \end{aligned}$$

Here the dependence of  $u$  on  $\Omega$  is unimportant and hence not indicated.

Differentiation shows that

$$(B.1) \quad \begin{aligned} \frac{\partial R}{\partial \rho} &= \int_0^{2\pi} R(\xi + \rho\sqrt{1+u(\theta)}e^{i\theta}, \xi + \rho\sqrt{1+u(\omega)}e^{i\omega})(1+u(\omega))\rho d\omega \\ &+ \int_{E_w} R_x(\xi + \rho\sqrt{1+u(\theta)}e^{i\theta}, y)[\sqrt{1+u(\theta)}e^{i\theta}] dy. \end{aligned}$$

From now on it is understood that in  $\sqrt{1+ue^{i\theta}}$ ,  $u$  is a function of  $\theta$  and in  $\sqrt{1+ue^{i\omega}}$ ,  $u$  is a function of  $\omega$ . Differentiation of (B.1) shows that

$$(B.2) \quad \begin{aligned} \frac{\partial^2 R}{\partial \rho^2} &= \int_0^{2\pi} R(\xi + \rho\sqrt{1+ue^{i\theta}}, \xi + \rho\sqrt{1+ue^{i\omega}})(1+u(\omega)) d\omega \\ &+ 2 \int_0^{2\pi} R_x(\xi + \rho\sqrt{1+ue^{i\theta}}, \xi + \rho\sqrt{1+ue^{i\omega}})[\sqrt{1+ue^{i\theta}}](1+u(\omega))\rho d\omega \\ &+ \int_0^{2\pi} R_y(\xi + \rho\sqrt{1+ue^{i\theta}}, \xi + \rho\sqrt{1+ue^{i\omega}})[(1+u)^{3/2}e^{i\omega}]\rho d\omega \\ &+ \int_{E_w} R_{xx}(\xi + \rho\sqrt{1+ue^{i\theta}}, y)[\sqrt{1+ue^{i\theta}}, \sqrt{1+ue^{i\theta}}] dy. \end{aligned}$$

Next

$$(B.3) \quad \begin{aligned} \frac{\partial^3 R}{\partial \rho^3} &= 3 \int_0^{2\pi} R_x(\xi + \rho\sqrt{1+ue^{i\theta}}, \xi + \rho\sqrt{1+ue^{i\omega}})[\sqrt{1+ue^{i\theta}}](1+u(\omega)) d\omega \\ &+ 2 \int_0^{2\pi} R_y(\xi + \rho\sqrt{1+ue^{i\theta}}, \xi + \rho\sqrt{1+ue^{i\omega}})[(1+u)^{3/2}e^{i\omega}] d\omega \\ &+ 3 \int_0^{2\pi} R_{xx}(\xi + \rho\sqrt{1+ue^{i\theta}}, \xi + \rho\sqrt{1+ue^{i\omega}})[\sqrt{1+ue^{i\theta}}, \sqrt{1+ue^{i\theta}}](1+u(\omega))\rho d\omega \\ &+ 2 \int_0^{2\pi} R_{xy}(\xi + \rho\sqrt{1+ue^{i\theta}}, \xi + \rho\sqrt{1+ue^{i\omega}})[\sqrt{1+ue^{i\theta}}, \sqrt{1+ue^{i\omega}}](1+u(\omega))\rho d\omega \\ &+ \int_0^{2\pi} R_{yx}(\xi + \rho\sqrt{1+ue^{i\theta}}, \xi + \rho\sqrt{1+ue^{i\omega}})[\sqrt{1+ue^{i\theta}}, \sqrt{1+ue^{i\omega}}](1+u(\omega))\rho d\omega \\ &+ \int_0^{2\pi} R_{yy}(\xi + \rho\sqrt{1+ue^{i\theta}}, \xi + \rho\sqrt{1+ue^{i\omega}})[\sqrt{1+ue^{i\omega}}, \sqrt{1+ue^{i\omega}}](1+u(\omega))\rho d\omega \\ &+ O(\rho^2). \end{aligned}$$

Finally we deduce

$$\begin{aligned}
 \frac{\partial^4 R}{\partial \rho^4} \Big|_{\rho=0} &= 12\pi R_{xx}(\xi, \xi)[\sqrt{1+ue^{i\theta}}, \sqrt{1+ue^{i\theta}}] \\
 &\quad + 5 \int_0^{2\pi} R_{xy}(\xi, \xi)[\sqrt{1+ue^{i\theta}}, \sqrt{1+ue^{i\omega}}](1+u(\omega)) d\omega \\
 &\quad + 3 \int_0^{2\pi} R_{yx}(\xi, \xi)[\sqrt{1+ue^{i\theta}}, \sqrt{1+ue^{i\omega}}](1+u(\omega)) d\omega \\
 &\quad + 3 \int_0^{2\pi} R_{yy}(\xi, \xi)[\sqrt{1+ue^{i\omega}}, \sqrt{1+ue^{i\omega}}](1+u(\omega)) d\omega \\
 &= 12\pi R_{xx}(\xi, \xi)[\sqrt{1+ue^{i\theta}}, \sqrt{1+ue^{i\theta}}] \\
 \text{(B.4)} \quad &\quad + 3 \int_0^{2\pi} R_{yy}(\xi, \xi)[\sqrt{1+ue^{i\omega}}, \sqrt{1+ue^{i\omega}}](1+u(\omega)) d\omega.
 \end{aligned}$$

REFERENCES

[1] F. S. BATES AND G. H. FREDRICKSON, *Block copolymers—designer soft materials*, Phys. Today, 52 (1999), pp. 32–38.

[2] X. CHEN AND Y. OSHITA, *Periodicity and uniqueness of global minimizers of an energy functional containing a long-range interaction*, SIAM J. Math. Anal., 37 (2006), pp. 1299–1332.

[3] M. DEL PINO, M. KOWALCZYK, AND J. WEI, *Concentration on curves for nonlinear Schrödinger equations*, Comm. Pure Appl. Math., 60 (2007), pp. 113–146.

[4] M. DEL PINO, M. KOWALCZYK, AND J. WEI, *Resonance and interior layers in an inhomogeneous phase transition model*, SIAM J. Math. Anal., 38 (2007), pp. 1542–1564.

[5] P. C. FIFE AND D. HILHORST, *The Nishiura–Ohnishi free boundary problem in the 1D case*, SIAM J. Math. Anal., 33 (2001), pp. 589–606.

[6] A. GIERER AND H. MEINHARDT, *A theory of biological pattern formation*, Kybernetik, 12 (1972), pp. 30–39.

[7] Z. HAN, *Asymptotic approach to singular solutions to nonlinear elliptic equations involving the critical Sobolev exponent*, Ann. Inst. H. Poincaré Anal. Non Linéaire, 8 (1991), pp. 159–174.

[8] T. KOLOKOLNIKOV, M. WARD, AND J. WEI, *Spot self-replication and dynamics for the Schnakenburg model in a two-dimensional domain*, J. Nonlinear Sci., 19 (2009), pp. 1–56.

[9] I. M. LIFSHITZ AND V. V. SLYOZOV, *The kinetics of precipitation from supersaturated solid solutions*, J. Phys. Chem. Solids, 19 (1961), pp. 35–50.

[10] B. NIETHAMMER, *Derivation of the LSW-theory for Ostwald ripening by homogenization methods*, Arch. Ration. Mech. Anal., 147 (1999), pp. 119–178.

[11] B. NIETHAMMER AND F. OTTO, *Ostwald ripening: The screening length revisited*, Calc. Var. Partial Differential Equations, 13 (2001), pp. 33–68.

[12] Y. NISHIURA AND I. OHNISHI, *Some mathematical aspects of the microphase separation in diblock copolymers*, Phys. D, 84 (1995), pp. 31–39.

[13] T. OHTA AND K. KAWASAKI, *Equilibrium morphology of block copolymer melts*, Macromolecules, 19 (1986), pp. 2621–2632.

[14] X. REN AND J. WEI, *Single-point condensation and least-energy solutions*, Proc. Amer. Math. Soc., 124 (1996), pp. 111–120.

[15] X. REN AND J. WEI, *On the multiplicity of solutions of two nonlocal variational problems*, SIAM J. Math. Anal., 31 (2000), pp. 909–924.

[16] X. REN AND J. WEI, *On energy minimizers of the di-block copolymer problem*, Interfaces Free Bound., 5 (2003), pp. 193–238.

[17] X. REN AND J. WEI, *Many droplet pattern in the cylindrical phase of diblock copolymer morphology*, Rev. Math. Phys., 19 (2007), pp. 879–921.

[18] X. REN AND J. WEI, *Single droplet pattern in the cylindrical phase of diblock copolymer morphology*, J. Nonlinear Sci., 17 (2007), pp. 471–503.

[19] X. REN AND J. WEI, *Spherical solutions to a nonlocal free boundary problem from diblock copolymer morphology*, SIAM J. Math. Anal., 39 (2008), pp. 1497–1535.

- [20] O. REY, *The role of the Green's function in a nonlinear elliptic equation involving the critical Sobolev exponent*, J. Funct. Anal., 89 (1990), pp. 1–52.
- [21] A. M. TURING, *The chemical basis of morphogenesis*, Phil. Transact. Royal Soc. B, 237 (1952), pp. 37–72.
- [22] C. WAGNER, *Theorie der Alterung von Niederschlägen durch Umlösen*, Z. Elektrochem., 65 (1961), pp. 581–594.